DOI: 10.1002/fuce.201200056

Fuel Cells

ORIGINAL RESEARCH PAPER

Modeling of a Tubular-SOFC: The Effect of the Thermal Radiation of Fuel Components and CO Participating in the Electrochemical Process

S. A. Hajimolana[1], M. A. Hussain[1]*, M. Soroush[2], W. M. A. Wan Daud[1], M. H. Chakrabarti[1]

[1] Department of Chemical Engineering, University of Malaya, 50603 Kuala Lumpur, Malaysia
[2] Department of Chemical and Biological Engineering, Drexel University, Philadelphia, Pennsylvania 19104, USA

Received April 08, 2012; accepted August 07, 2012

Abstract

A mathematical model based on first principles is developed to study the effect of heat and electrochemical phenomena on a tubul solid oxide fuel cell (SOFC). The model accounts fordiffusion, inherent impedance, transport (momentum, heat and mass transfer) processes, internal reforming/shifting reaction, electrochemical processes, and potential losses (activation, concentration, and ohmic losses). Thermal radiation of fuel gaseous components is considered in detail in this work in contrast to other reported work in the literature. The effect of thermal radiation on SOFC performance is shown by comparing with a model without this factor. Simulation results indicate that at higher inlet fuel flow pressures and also larger SOFC lengths the effect of thermal radiation on SOFC temperature becomes more significant. In this study, the H_2 and CO oxidation is also studied and the effect of CO oxidation on SOFC performance is reported. The results show that the model which accounts for the electrochemical reaction ofCO results in better SOFC performance than other reported models. This work also reveals that at low inlet fuel flow pressures the CO and H_2 electrochemical reactions are competitive and significantly dependent on the CO/H_2 ratio inside the triple phase boundary.

Keywords: Cell-tube Temperature, CO Oxidation, Outlet Voltage, SOFC, Thermal Radiation of Fuel Gas Components

1 Introduction

Solid oxide fuel cells (SOFCs) are promising electricity production sources for stationary applications and power generation in the short- to medium-term future. This is due to the high energy efficiency achieved in a SOFC, which tends to be much higher than that generated from conventional heat engines or other types of fuel cells [1, 2]. SOFC may work with several common hydrocarbon fuels such as natural gas, diesel, gasoline, and alcohol without the necessity of reforming the fuel into pure hydrogen. Another key advantage of the SOFC stems from its high operating temperature, due to which it possesses inherently rapid electrode kinetics and requires less catalysts to improve its efficiency thereby enabling it to operate with CO, which can be a poison to other types of fuel cells [3]. This is especially so for the polymer electrolyte fuel cell.

Mathematical modeling is an essential tool for designing fuel cell systems which represents the important aspects of the existing system and presents knowledge of that system in a useful manner. There have been several publications, studying the effect of different variables and their sensitivity on the SOFC performance [4–8, 59]. The reported works described SOFC's steady-state or dynamic performances. Such models have represented different geometries (planar, tubular, micro), positive-electrodes/electrolyte/negative-electrode structures (electrolyte or electrode-supported), flow configurations (cross-, co-, or counter- flow), modeling ranges from 0 to three-dimensions. The models also

[*] *Corresponding author, mohd_azlan@um.edu.my*

account for the provision of different fuels (hydrocarbons, syngas, hydrogen, and ammonia) [1, 5, 8–25]. Variable phenomena play an important role in the SOFC performance. However, it is not yet clear which of thephenomena are significant in a particular design and a given operating region. After a modeling approach is selected, significant simplifications are typically made to solve the model equations. It is quite possible that the accuracy that is expected from a detailed model is greatly reduced because of these simplifications and the impact of these simplifications on the predictive capability of the model is usually not clearly understood.

It is observed in all models that have considered the thermal effects the material properties, chemical kinetics, and transport properties of materials used in a single cell and stack depend on the temperature. Therefore, it is essential to develop a heat transfer model that could account for various heat effects in both of the solid structures and the flow channels in order to have an accurate prediction of fuel cell behavior. Because of the high operating temperatures of SOFCs, thermal radiation is an important factor of heat transfer within them. Thermal radiation has been accounted for by many researchers [26–30], but some researchers ignored thermal radiation because they considered uniform temperature throughout the cell [31, 32], or due to the assumption of thin walled channels [33]. Moreover, the thermal radiation between the walls and gas components is not accounted for in the literature while those from the fuel components including H_2O, CH_4, CO, CO_2, and possibly other hydrocarbons in high operating temperatures exhibit spectral, temperature, and pressure dependencies due to which they can be treated transparently [34]. On the other hand, fuel cell temperature and outlet voltage depend highly on the electrochemical reactions. When both H_2 and CO are present in the SOFC, current is produced from the sum of hydrogen and carbon monoxide oxidation at the anode by means of an electrochemical reaction. CO oxidation influences the overall performance of the cell and on the other hand, polarization losses have an impact upon outlet voltage directly. In many studies, CO oxidation in electrochemical reactions is neglected or polarization losses are not completely accounted for [19, 30, 35–45]. Hofman et al. [46] assumed that when both species of H_2 and CO are present in the system, CO mostly participates in the water–gas shift reaction rather than in the electrochemical process due to its fast kinetics. However, it is not quite clear how these simplified assumptions for the electrochemical modeling can influence the accuracy of the model. On the other hand, some other researchers considered the CO electrochemical reaction in their system. Petruzzi et al. [47] developed two different approaches. In the first one only the water shift reaction of CO was considered, while in the second one both the electrochemical oxidation of CO and the shift reaction were taken into account. Results from these two extreme approaches were compared. It was observed that CO oxidation at the electrochemical reaction influenced the cell efficiency, fuel utilization, thermodynamic efficiency, and electric power. However, the authors [15, 22] neglected concentration polarization and diffusional mass transfer in their study, while such phenomena should have been taken into account if the contribution of the CO electrochemical reaction was meant to be considered. Ho et al. [19] also accounted for CO electrochemical reaction in their model at an oxidation rate of three times less than that of H_2 since the operating temperature of the fuel cell was high (800–1,000 °C). But the electromotive force calculation was based only on H_2 oxidation and the concentration polarization was not accounted for in their study. In another study, Aloui and Halouani [48] compared the fuel cell performance with and without carbon monoxide oxidation at the anode. It was reported that SOFC fuelled with a mixture of CO and H_2 was more powerful compared to the pure H_2 fed SOFC if the CO electrochemical reaction was taken into fully account. The study was based on an analytical model for calculation in polarization of fuel cell; while the model did not consider the entire system, and did not account for the momentum and heat balances. Khaleel et al. [3] presented a 3D simulation tool for modeling a SOFC. However, the momentum balance was also not accounted for and the heat transfer was not considered in sufficient detail in their study. They proposed an *I–V* model for H_2 fuel and also an *I–V* model for fuel having CO. It was estimated that the activation polarization for H_2 and CO was the same. The competition of H_2 and CO oxidation was not clearly shown in their study and the effect of CO electrochemical reaction on fuel cell was not clear.

In this paper, a dynamic compartmental model based on firstprinciples is developed. The dynamic model accounts for the diffusion process, inherent impedance, transport (momentum, heat and mass transfer) processes, and internal reforming/shifting reaction, as well as electrochemical processes, and potential losses including activation, concentration and ohmic losses, among others. Accounting for the thermal radiation of gaseous components is a missing factor in most SOFC models while in this work these factors are considered in detail and this effect on fuel cell temperature is studied. In this work, H_2 and CO oxidation is also studied and the effect of CO oxidation on outlet fuel cell voltage is investigated.

The organization of this paper is as follows. Section 2 describes the SOFC dynamic model in details, and Section 3 presents the results from the modeling study and discusses the importance of thermal radiation of gaseous components and CO electrochemical reaction inside the model. Concluding remarks are presented in Section 4.

2 Model Description

Fuel cell modeling is implemented for research and in the industry in order to develop new materials, system layouts, and cell assemblies. A precise analytical study previous to testing saves a considerable amount of money, as fuel cell testing is expensive and time consuming. It is therefore essential that the model for this purpose generates meaningful results. This work is aimed at assessing the impact of the ther-

mal radiation of gaseous components on the fuel cell temperature. Also this work, studies the effect of the electrochemical reaction of CO on fuel cell performance. The SOFC system under study consists of a single tubular SOFCs. Each cell contains two tubes, an outer and an inner tube, and this is illustrated in Figure 1. The outer one is a cell tube. The outer surface of the outer tube is represented as the anodic side of the cell and its inner surface is considered as the cathode side. Between the anodic and cathode sides (surfaces) lies the solid oxide electrolyte. The inner tube has an air injection and guidance tube, which is composed of alumina, from which preheated air is injected into the bottom of the cell tube and flows over the cathode surface through the gap between the injection tube and the cell tube. Fuel gas flows over the anode surface through the gap amongst the cell tubes. The key geometric dimensions are summarized in Table 1.

Table 1 Parameters used in the simulation.

Parameter	Value	References
A_{ano}	3.922×10^{-5} m^2	
r_{cto}	1.1×10^{-2} m	[29]
r_{cti}	8.66×10^{-3} m	[29]
r_{ito}	6×10^{-3} m	[29]
r_{iti}	5×10^{-3} m	[29]
L	5×10^{-2} m	[29]
m_{ct}	3.317×10^{-2} kg	
m_{it}	6.735×10^{-3} kg	
C_{ct}	3×10^{-1} *A S V*	[29]
R_{tct}	9×10^{-1} Ω	[29]
R_{to}	1×10^{-1} Ω	[29]
$\tilde{C}_{p_{ct}}$	7.4×10^{-1} kJ kg^{-1} K^{-1}	[29]
$\tilde{C}_{p_{it}}$	$0.9768 + 0.000241 \times T_{it}$ kJ/(kg K)	[29]
ε_{cat}	5.0×10^{-1}	[29]
τ_{cat}	3.0×10^{0}	[29]
ε_{ano}	5.0×10^{-1}	[29]
τ_{ano}	3.0×10^{0}	[29]
Δ_{ano}	1.0×10^{-4} m	[29]
Δ_{cat}	2.21×10^{-4} m	[29]
$E_{act_{ano}}$	1.10×10^{5} kJ kmol^{-1}	[29]
$E_{act_{cat}}$	1.20×10^{5} kJ kmol^{-1}	[29]
δ_{ano}	5.0×10^{-7} m	[11]
δ_{cat}	5.0×10^{-7} m	[11]

To develop a first-principles model of the SOFC system, a single tubular fuel cell is considered and divided into five subsystems, as shown in Figure 1. Subsystem 1 (SS1) consists of air inside the injection tube, Subsystem 2 (SS2) is a solid injection tube, Subsystem 3 (SS3) consists of air inside the space between the cell and injection tubes, Subsystem 4 (SS4) is represented by the cell tube, and finally Subsystem 5 (SS5) consists of the fuel flow channel.

The fuel cell model is derived by writing mass, energy, and/or momentum conservation equations for each of the five subsystems. The assumption considered in the mathematical formulation is that the gaseous boundary layers are very small relative to the corresponding radius; therefore, the equations governing the diffusion process are in form of the Cartesian coordinates. Fluid velocities, temperatures, and pressures are averaged along the radial direction. Specific properties such as conductivities, heat capacities, viscosities, and densities in each subsystem are also uniform. Furthermore, output partial pressures, temperatures, and velocities are equal to the pressures, temperatures, and velocities inside the subsystem. The external load (resistances) of the cell is considered to be pure resistance. Table 2 presents the values used as the operating condition.

Table 2 Operating conditions of the model.

Parameter	Value	References
R_{load}	4 Ω	
$P^{ano}_{fuel_{in}}$	1 atm.	[29]
$T^{ano}_{fuel_{in}}$	823 K	[29]
$u^{ano}_{fuel_{in}}$	0.927 m s^{-1}	[29]
$\xi^{ano}_{CH_{4in}}$	0.0248	[53]
$\xi^{ano}_{H_2O_{in}}$	0.0273	[53]
$\xi^{ano}_{H_{2in}}$	0.5915	[53]
$\xi^{ano}_{CO_{in}}$	0.3550	[53]
$\xi^{ano}_{CO_{2in}}$	0.0014	[53]
$\xi^{ano}_{O_{2in}}$	0.2333	[53]
$P^{inj}_{air_{in}}$	1 atm.	[32]
$T^{inj}_{air_{in}}$	1,104 K	[32]
$u^{inj}_{air_{in}}$	450 m s^{-1}	

2.1 Dynamic Equations for Subsystem 1 (SS1)

This subsystem includes the air inside the injection tube. The mass/momentum and energy balances inside SS1 are given as follows:

$$L\frac{\mathrm{d}\rho^{inj}_{air}}{\mathrm{d}t} = u^{inj}_{air_{in}}\rho^{inj}_{air_{in}} - u^{inj}_{air}\rho^{inj}_{air} \tag{1}$$

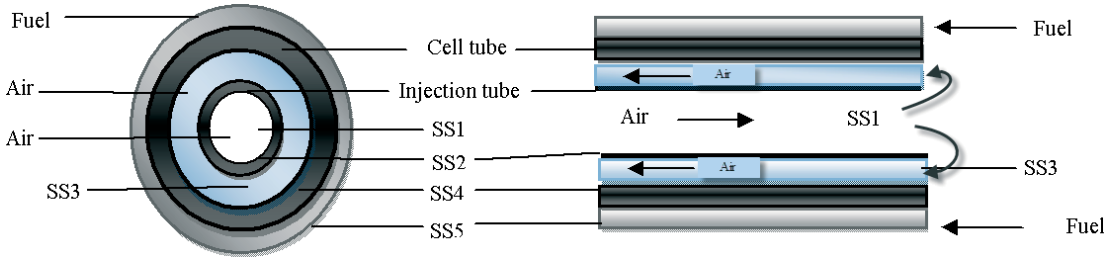

Fig. 1 Division of the single tubular SOFC into five subsystems.

$$L\frac{\mathrm{d}(u_{air}^{inj}\rho_{air}^{inj})}{\mathrm{d}t} = (u_{air_{in}}^{inj})^2\rho_{air_{in}}^{inj} - (u_{air}^{inj})^2\rho_{air}^{inj} + \frac{\rho_{air_{in}}^{inj}R^*T_{air_{in}}^{inj}}{M_{air}} - \frac{\rho_{air}^{inj}R^*T_{air}^{inj}}{M_{air}} \quad (2)$$

$$L\frac{\mathrm{d}(\tilde{H}_{air}^{inj}\rho_{air}^{inj})}{\partial t} = u_{air_{in}}^{inj}\rho_{air_{in}}^{inj}H_{air_{in}}^{inj} - u_{air}^{inj}\rho_{air}^{inj}\tilde{H}_{air}^{inj} + \frac{2Lh_{it_i}}{r_{it_i}} \times \left(T_{it} - T_{air}^{inj}\right) \quad (3)$$

This model assumes that the pressure drop caused by the injection pipe resistance over the distance L is negligible. Enthalpy of formation, heat capacities, viscosities, convection heat transfer coefficients, and conductivities of the components of air and the fuel are given in a previous work [26].

2.2 Dynamic Equations for Subsystem 2 (SS2)

Subsystem 2 is the solid injection tube. An energy balance for the injection tube leads to

$$m_{it}\tilde{C}_{p_{it}}\frac{\mathrm{d}T_{it}}{\mathrm{d}t} = \frac{\sigma 2\pi r_{it_o}L}{R_{rad}}\left(T_{ct}^4 - T_{it}^4\right) + 2\pi r_{it_o}Lh_{it_o}(T_{air}^{cat} - T_{it}) + 2\pi r_{it_i}Lh_{it_i}\left(T_{air}^{inj} - T_{it}\right) \quad (4)$$

2.3 Dynamic Equations Subsystem 3 (SS3)

Subsystem 3 consists of the air (including oxygen and nitrogen) that flows inside the space between the injection tube outer surface and the cathode (inner) surface of the cell tube. From this subsystem, O_2 diffuses into the cell tube. A mass, momentum and energy balance on the air inside SS3 takes the following form, respectively:

Mass balance on oxygen inside SS3:

$$L\frac{\mathrm{d}\left(\rho_{air}^{cat}\tilde{\zeta}_{O_2}^{cat}\right)}{\mathrm{d}t} = u_{air_{in}}^{cat}\rho_{air_{in}}^{cat}\tilde{\zeta}_{O_{2_{in}}}^{cat} - u_{air}^{cat}\rho_{air}^{cat}\tilde{\zeta}_{O_2}^{cat} - N_{O_2}M_{O_2}\left(\frac{2r_{ct_i}L}{r_{ct_i}^2 - r_{it_o}^2}\right) \quad (5)$$

A momentum balance on the air inside SS3 is

$$L\frac{\mathrm{d}(u_{air}^{cat}\rho_{air}^{cat})}{\mathrm{d}t} = (u_{air_{in}}^{cat})^2\rho_{air_{in}}^{cat} - (u_{air}^{cat})^2\rho_{air}^{cat} + \frac{\rho_{air_{in}}^{cat}R^*T_{air_{in}}^{cat}}{M_{air}} - \frac{\rho_{air}^{cat}R^*T_{air}^{cat}}{M_{air}^{cat}} \quad (6)$$

An energy balance on SS3 is given by

$$L\frac{\mathrm{d}(\tilde{H}_{air}^{cat}\rho_{air}^{cat})}{\partial t} = u_{air_{in}}^{cat}\rho_{air_{in}}^{cat}\tilde{H}_{air_{in}}^{cat} - u_{air}^{cat}\rho_{air}^{cat}\tilde{H}_{air}^{cat} + \frac{2r_{it_o}Lh_{it_o}}{r_{ct_i}^2 - r_{it_o}^2}(T_{it} - T_{air}^{cat}) - \frac{2r_{ct_i}Lh_{ct_i}}{r_{ct_i}^2 - r_{it_o}^2}(T_{ct} - T_{air}^{cat}) - N_{O_2}\tilde{H}_{air}^{cat}\left(\frac{2r_{ct_i}L}{r_{ct_i}^2 - r_{it_o}^2}\right) \quad (7)$$

2.4 Dynamic Equations for Subsystem 4 (SS4)

Fuel cell tube (SS4) consists of the anode layer, the cathode layer and the electrolyte layer in between them. In this subsystem energy balance and diffusional mass balance can be accounted for this subsystem. Electrochemical reactions, shift and reforming reactions are also adequately covered in this subsystem. Shift and reforming reactions occur on the anode surface layer that are discussed in detail in Ref. [26].

2.4.1 Energy Balance

The heat transfer and energy sources that are considered in the fuel cell-tube involving convection/radiation heat transfer, diffusional heat transfer, heating produced by H_2 and CO oxidations, heating consumed by the reforming reaction, and heat produced by the shift reaction. Based on the heat transfer considered in this model an energy balance for this subsystem yields:

$$\mathrm{m}_{ct}C_{pct}\frac{\mathrm{d}T_{ct}}{\mathrm{d}t} = H + 2r_{ct_i}Lh_{ct_i}\left(T_{air}^{cat} - T_{ct}\right) + 2r_{ct_o}Lh_{ct_o}\left(T_{fuel}^{ano} - T_{ct}\right) + \frac{\sigma 2\pi r_{ct_i}L}{R_{rad}}\left(T_{it}^4 - T_{ct}^4\right) + Q_{rad}^{comp} + 2r_{ct_o}LR_{ref}\Delta H_{ref} + 2r_{ct_o}LR_s\Delta H_s + Q_{Oxy_{H_2}} + Q_{Oxy_{CO}} \quad (8)$$

where H is the heat transfer diffusing by the components in/out of the triple phase boundary (TPB), given by:

$$H = 2\pi L\begin{pmatrix} r_{ct_i}N_{O_2}H_{O_2}^{cat} + r_{ct_o}N_{H_2}H_{H_2}^{ano} - \\ r_{ct_o}N_{H_2O}H_{H_2O}^{ano} + r_{ct_o}N_{CO}H_{CO}^{ano} - \\ r_{ct_o}N_{CO_2}H_{CO_2}^{ano} \end{pmatrix} \quad (9)$$

The second and third terms of the energy balance (Eq. 8) are heat transfer by means of convection between the cell-tube and air flow in SS3 and the cell tube and fuel flow in SS5, respectively. The forth term is the thermal radiation between the inner cell tube surface and the outer injection tube surface while ΔH_{ref} and ΔH_s are the heat released by the reactions while R_{ref} and R_s are the rate of reforming and shift reactions, respectively. The heats produced by electrochemical oxidations are given as follows:

$$Q_{Oxy_{H_2}} = R_{H_2O}H_{H_2O}^{ct} - R_{H_2}H_{H_2}^{ct} - \frac{1}{2}R_{O_2}H_{O_2}^{ct} \quad (10)$$

$$Q_{Oxy_{CO}} = R_{CO_2}H_{CO_2}^{ct} - R_{CO}H_{CO}^{ct} - \frac{1}{2}R_{O_2}H_{O_2}^{ct} \quad (11)$$

Q_{rad}^{comp} is the thermal radiation between the fuel components and the outer cell tube surface. Fuel components inclusive of H_2O, CH_4, CO, CO_2 and possibly other hydrocarbons are spectral, temperature and pressure dependencies and thus can be treated transparently [34].

The calculation of thermal radiation exchange is simplified by assuming that each of the gaseous components is considered to be a gray gas [34]. It is possible to represent the real gaseous components by a weighted sum of gray gases along with a clear gas. This heat transfer is evaluated by using Eq. (13):

$$q_{rad,comp} = \frac{\varepsilon_w}{1-(1-a_g)(1-\varepsilon_w)}\sigma(\varepsilon_g T_{fuel}^{ano4} - a_g T_{ct}^4) \quad (12)$$

where the emissivity (ε_g) of a gray gas is given by [49]:

$$\varepsilon_{g_i} = 1 - \exp(-k_g P_i L) \quad (13)$$

where k_g is the absorption coefficient (m^{-1} atm^{-1}), P_i is the partial pressure (atm) of the absorbing gas, and L is the beam length.

The total emissivity of a real gas (ε_g) can be represented mathematically by a mixture of N gray gaseous components of different absorption coefficients, $k_{g,n}$ [50]:

$$\varepsilon_g = \sum a_{g,n}\left[1 - \exp(-k_{g,n}P_i L)\right] \quad \text{for} \quad n = 1, N \quad (14)$$

where $a_{g,n}$ are the weighted coefficients for each gray gaseous component.

In general, one of the gases is assumed to be transparent with an absorption coefficient (k_g) of 0. Here, $a_{g,n}$ is simply given as [51]:

$$a_{g,n} = b_{1,n} + b_{2,n}\, T_{fuel} \quad (15)$$

where $b_{1,n}$ and $b_{2,n}$ are constants and T_{fuel} is the gas temperature.

The data for a simple model having four terms representing a natural gas is reproduced from Ref. [50] in Table 3.

Table 3 Mixed gray-gas model parameters for natural gas combustion products.

N	$b_{1,n}$	$b_{2,n}$	$k_{g,n}$
1	0.423	0.0433×10^{-3}	0
2	0.285	0.0513×10^{-3}	0.89
3	0.227	-0.0676×10^{-3}	15.5
4	0.065	-0.027×10^{-3}	240.0

A four-term (three gray plus one clear) gas model is reproduced here [50].

A gas absorptivity model which provides satisfactory accuracy is given by [52]:

$$a_g = \sum a_{s,n}\left(\frac{T_{fuel}^{ano}}{T_{ct}}\right) \quad (16)$$

where

$$a_{s,n} = b_{1,n} + b_{2,n}T_{ct} \quad (17)$$

2.4.2 Electrochemical Model

Voltage and current are produced by the electrochemical reactions occurring inside the TPB. At the cathode side oxygen ions (with a negative charge) migrate through the crystal lattice. The oxygen is supplied, from air, at the cathode while H_2 and CO in the fuel stream, diffuse into the anodic side and react at the TPB with oxide ions (O^{2-}) from the electrolyte to produce steam and CO_2 and deposit electrons at the anode. The electrons pass outside the fuel cell, through the resistance, and back to the cathode, where oxygen from the air receives the electrons and is converted to oxide ions, which are then injected into the electrolyte. Generating efficiencies can range up to 60%. The high operating temperature of the SOFC offers the possibility of internal reforming. The SOFC electrochemical reactions inside the TPB can be described as:

$$\text{Anodic Side Rections} \begin{cases} H_2 + O^{2-} \rightarrow H_2O + 2e & (a) \\ CO + O^{2-} \rightarrow CO_2 + 2e & (b) \end{cases}$$

$$\text{Cathodic Side Reaction} \left\{ O_2(g) + 4e \longrightarrow 2O^{2-} \quad (c) \right.$$

It should be note that a SOFC can use CO as well as hydrogen as its direct fuel. There are two approaches for calculating the potential across the electrolyte (as shown in Figure 2). In Figure 2a, only H_2 oxidation has been considered. In this approach the relations between current and potential across the electrolyte follows the series circuit rule.

However, according to the second approach (as shown in Figure 2b) both H_2 and CO oxidation has to be considered. In this approach the relationship between potential and current follows the parallel circuit rule. For this feature the Nernst potentials for reactions (a) and (b) are given respectively by:

$$E_{H_2} = E^0_{H_2} + \frac{R_J T_{ct}}{2F} \ln\left[\frac{P^{TPB}_{H_2}(P^{TPB}_{O_2})^{1/2}}{P^{TPB}_{H_2O}}\right] \quad (18)$$

and

$$E_{CO} = E^0_{CO} + \frac{R_J T_{ct}}{2F} \ln\left[\frac{P^{TPB}_{CO}(P^{TPB}_{O_2})^{1/2}}{P^{TPB}_{CO_2}}\right] \quad (19)$$

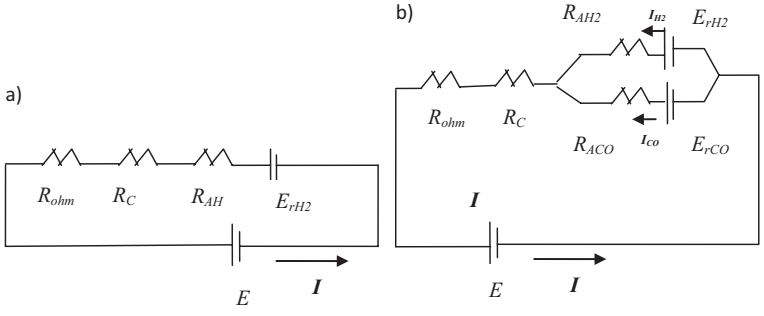

Fig. 2 Two approaches for calculating the potential across the electrolyte.

However, the actual cell voltage (E) is less than its theoretical open circuit voltage because it is strongly affected by several irreversible losses. These include activation losses due to irreversibility of electrochemical reactions at the TPB, concentration losses due to mass transport resistance in the electrodes with thick anodes as in an anode-supported SOFC and ohmic losses due to ionic and electronic charge transfer resistances. The actual cell voltage is given by:

$$E = E_{H_2} - \eta_{act_{H_2}} - \eta_{conc_{H_2}} - \eta_{act_{O_2}} - \eta_{conc_{O_2}} - \eta_{ohm} \tag{20}$$

and

$$E = E_{CO} - \eta_{act_{CO}} - \eta_{conc_{CO}} - \eta_{act_{O_2}} - \eta_{conc_{O_2}} - \eta_{ohm} \tag{21}$$

Current is produced by the sum of H_2 and CO oxidation at the anodic side by electrochemical reaction where it is assumed that the rate of H_2 oxidation is 2.5 times more than that of the CO oxidation [53]. The total current density is given by:

$$\begin{aligned} I_{tot} &= I_{o_2} \\ I_{tot} &= I_{H_2} + I_{CO} \end{aligned} \tag{22}$$

2.4.3 Polarizations

The activation polarizations are the result of the kinetics involved with the electrochemical reactions. It becomes important for accounting in the model when the current is low, because at low current the reactants must overcome an energy barrier that is known as the activation energy (E_{act}) in order to drive the electrochemical reactions at the electrodes–electrolyte interface and this barrier leads to the polarization. The activation barrier is the result of many complex electrochemical reaction steps where, typically, the rate-limiting step is responsible for the polarization. A linear approach is applicable if the equilibrium potential change is small. Anodic and cathodic activation polarizations are calculated for every segmented volume [27] as follows:

$$\eta_{act_{H_2}} = \left[\frac{4F}{R_J T_{ct}} k_{act_{H_2}} \left(\frac{P_{H_2}^{TPB}}{P^0}\right)^{0.25} \left(-\frac{E_{act_{ano}}}{R_{KJ} T_{ct}}\right)\right]^{-1} \times I_{H_2} \tag{23}$$

$$\eta_{act_{CO}} = \left[\frac{4F}{R_J T_{ct}} k_{act_{CO}} \left(\frac{P_{CO}^{TPB}}{P^0}\right)^{0.25} \left(-\frac{E_{act_{ano}}}{R_{KJ} T_{ct}}\right)\right]^{-1} \times I_{CO} \tag{24}$$

$$\eta_{act_{O_2}} = \left[\frac{4F}{R_J T_{ct}} k_{act_{O_2}} \left(\frac{P_{O_2}^{TPB}}{P^0}\right)^{0.25} \left(-\frac{E_{act_{cat}}}{R_{KJ} T_{ct}}\right)\right]^{-1} \times I \tag{25}$$

Concentration losses are losses associated with concentration variation of the critical (active electrochemical) species due to mass transport processes. There are usually two sources for the mass transport: (i) diffusion between the bulk flow and cell surfaces, and (ii) transport of reactants and products through electrodes. Therefore, the concentration polarization is highly dependent on the gases used, as well as the distance through which the gases must diffuse. Pore volume percentage, as well as diffusion length, can be varied to optimize these properties. For similar geometries, cathode concentrations are much larger than anode concentrations, because of the lower diffusivities of O_2/N_2 in the cathode than H_2/H_2O in the anode. The anodic and cathode concentration losses can be calculated respectively as follows:

$$\eta_{conc_{H_2}} = \frac{R_J T_{ct}}{2F} \ln\left(\frac{P_{H_2} P_{H_2O}^{TPB}}{P_{H_2}^{TPB} P_{H_2O}}\right) \tag{26}$$

$$\eta_{conc_{CO}} = \frac{R_J T_{ct}}{2F} \ln\left(\frac{P_{CO} P_{CO_2}^{TPB}}{P_{CO}^{TPB} P_{CO_2}}\right) \tag{27}$$

$$\eta_{conc_{O_2}} = \frac{R_J T_{ct}}{4F} \ln\left(\frac{P_{O_2}}{P_{O_2}^{TPB}}\right) \tag{28}$$

An approximate equivalent circuit of a SOFC that consists of two internal resistances and one internal capacitance is given in a separate publication [26, 54]. According to the equivalent circuit approximation, the cell outlet voltage is governed by the following equations:

$$\begin{aligned} \frac{dV_{tl}}{dt} &= \left(\frac{1}{R_{tct} C_{ct}}\right) E - \frac{1}{C_{ct}} \left(\frac{1}{R_{tct}} + \frac{1}{R_{to} + R_{load}}\right) V_{tl} \\ V_{out} &= \left(\frac{R_{load}}{R_{to} + R_{load}}\right) V_{tl} \\ I &= \left(\frac{1}{R_{to} + R_{load}}\right) V_{tl} \end{aligned} \tag{29}$$

where R_{to} is the total ohmic resistance representing the inherent impedance of the cell, R_{tct} is the total charge transfer resistance of the cell, C_{ct} is the charge transfer capacitance of the cell, I is the current through the external resistive load, V_{out} is the fuel cell outlet voltage (voltage across the external load), and V_{tl} is the voltage across the total ohmic resistance and the load resistance in series.

2.4.4 Model Equations for the Cathode and Anodic-side Diffusion Layer in SS4

O_2 diffuses from SS3 into the cathodic side of the cell tube. A mole balance on oxygen inside the cathodic-side diffusion layer yields:

$$\frac{\Delta_{cat}}{R} \frac{d}{dt}\left[\frac{P_{O_2}^{TPB}}{T_{ct}}\right] = N_{O_2} - \left(\frac{1}{2\pi r_{ct_i} L}\right) R_{O_2} \tag{30}$$

On the other side H_2 and CO diffuse from the fuel flow channel into the anodic side of the cell tube whereas H_2O and CO_2 diffuse from the anodic side of the cell tube into the fuel flow channel. Mole balances on H_2, CO, H_2O, and CO_2 inside the anodic-side diffusion layers are given as follows:

$$\frac{\Delta_{ano}}{R}\frac{\mathrm{d}}{\mathrm{d}t}\left[\frac{P^{TPB}_{H_2}}{T_{ct}}\right] = N_{H_2} - \left(\frac{1}{2\pi r_{ct_o} L}\right)R_{H_2} \quad (31)$$

$$\frac{\Delta_{ano}}{R}\frac{\mathrm{d}}{\mathrm{d}t}\left[\frac{P^{TPB}_{H_2O}}{T_{ct}}\right] = -N_{H_2O} + \left(\frac{1}{2\pi r_{ct_o} L}\right)R_{H_2O} \quad (32)$$

$$\frac{\Delta_{ano}}{R}\frac{\mathrm{d}}{\mathrm{d}t}\left[\frac{P^{TPB}_{CO}}{T_{ct}}\right] = N_{CO} - \left(\frac{1}{2\pi r_{ct_o} L}\right)R_{CO} \quad (33)$$

$$\frac{\Delta_{ano}}{R}\frac{\mathrm{d}}{\mathrm{d}t}\left[\frac{P^{TPB}_{CO_2}}{T_{ct}}\right] = -N_{CO_2} + \left(\frac{1}{2\pi r_{ct_o} L}\right)R_{CO_2} \quad (34)$$

It is assumed that the rate of H_2 oxidation is 2.5 times more than that of the CO oxidation [53]. The rates of consumption of H_2, CO, and O_2 by the electrochemical reactions to generate an electric current of I are given by the following equations:

$$R_{H_2} = \left(\frac{1}{2F}\right)\times(0.714I) \quad (35)$$

$$R_{H_2} = \left(\frac{1}{2F}\right)\times(0.714I) \quad (36)$$

$$R_{CO} = \left(\frac{1}{2F}\right)(0.284I) \quad (37)$$

$$R_{O_2} = \left(\frac{1}{4F}\right)I \quad (38)$$

The consumption of the reactants is accompanied by the production of water at the following rates:

$$R_{H_2O} = -\left(\frac{1}{2F}\right)\times(0.714I) \quad (39)$$

$$R_{CO_2} = -\left(\frac{1}{2F}\right)(0.284I) \quad (40)$$

The rate of mass transfer of components is discussed in detail in Ref. [26]. The effective gas diffusion coefficient for components in the porous media can be defined as follows [9, 59]:

$$D_{H_2e} = \frac{\varepsilon_{ano}}{\tau_{ano}}\left(\frac{1-a_{H_2m}\zeta_{H_2}}{D_{H_2,m}} + \frac{1}{D_{K,H_2}}\right)^{-1} D_{H_2Oe}$$
$$= \frac{\varepsilon_{ano}}{\tau_{ano}}\left(\frac{1-a_{H_2Om}\zeta_{H_2O}}{D_{H_2O,m}} + \frac{1}{D_{K,H_2O}}\right)^{-1}$$

$$D_{COe} = \frac{\varepsilon_{ano}}{\tau_{ano}}\left(\frac{1-a_{COm}\zeta_{CO}}{D_{CO,m}} + \frac{1}{D_{K,CO}}\right)^{-1} D_{CO_2e}$$
$$= \frac{\varepsilon_{ano}}{\tau_{ano}}\left(\frac{1-a_{CO_2,m}\zeta_{CO_2}}{D_{CO_2,m}} + \frac{1}{D_{K,CO_2}}\right)^{-1} \quad (41)$$

where ε_{ano} is the volume fraction of anodic pores, τ_{ano} is the anodic tortuosity factor, ξ is the molar fraction, and $a_{i,m}$ is defined as [58]:

$$a_{H_2,m} = 1 - \left(\frac{M_{H_2}}{M_m}\right)^{1/2} \quad a_{H_2O,m} = 1 - \left(\frac{M_{H_2O}}{M_m}\right)^{1/2}$$

$$a_{CO,m} = 1 - \left(\frac{M_{CO}}{M_m}\right)^{1/2} \quad a_{CO_2,m} = 1 - \left(\frac{M_{CO_2}}{M_m}\right)^{1/2} \quad (42)$$

M_m is the average molecular weight represented as:

$$M_m = \xi_{H_2O}M_{H_2O} + \xi_{H_2}M_{H_2} + \xi_{CO}M_{CO} + \xi_{CO_2}M_{CO_2}$$

In a multi component gaseous system, the Knudsen diffusion coefficient, molecular diffusion coefficient of the components and the binary diffusion coefficient using the Fuller correlation [55] are given in Table 4.

Table 4 Diffusion coefficients of components accounted for in the model.

Knudsen diffusion coefficient of components:

$$D_{K,H_2} = 97\delta_{ano}\sqrt{\frac{T_{ct}}{M_{H_2}}} \quad D_{K,H_2O} = 97\delta_{ano}\sqrt{\frac{T_{ct}}{M_{H_2O}}}$$

$$D_{K,CO} = 97\delta_{ano}\sqrt{\frac{T_{ct}}{M_{CO}}} \quad D_{K,CO_2} = 97\delta_{ano}\sqrt{\frac{T_{ct}}{M_{CO_2}}}$$

M is the molar weight of components

Molecular diffusion coefficient [9]:

$$D_{H_2,m} = \frac{1-\zeta_{H_2}}{\frac{\zeta_{H_2O}}{D_{H_2-H_2O}} + \frac{\zeta_{CO}}{D_{H_2-CO}} + \frac{\zeta_{CO_2}}{D_{H_2-CO_2}}} \quad D_{H_2O,m} = \frac{1-\zeta_{H_2O}}{\frac{\zeta_{H_2}}{D_{H_2-H_2O}} + \frac{\zeta_{CO}}{D_{H_2O-CO}} + \frac{\zeta_{CO_2}}{D_{H_2O-CO_2}}}$$

$$D_{CO,m} = \frac{1-\zeta_{CO}}{\frac{\zeta_{H_2}}{D_{H_2-CO}} + \frac{\zeta_{H_2O}}{D_{H_2O-CO}} + \frac{\zeta_{CO_2}}{D_{CO-CO_2}}} \quad D_{CO_2,m} = \frac{1-\zeta_{CO_2}}{\frac{\zeta_{H_2}}{D_{H_2-CO_2}} + \frac{\zeta_{H_2O}}{D_{H_2O-CO_2}} + \frac{\zeta_{CO}}{D_{CO-CO_2}}}$$

Binary diffusion coefficient:

$$D_{H_2-H_2O} = \frac{1.013\times10^{-7}T_{ct}^{1.75}[(1/M_{H_2}) + (1/M_{H_2O})]^{1/2}}{[P^{TPB}_{H_2} + P^{TPB}_{H_2O} + P^{TPB}_{CO} + P^{TPB}_{CO_2}](v_{H_2}{}^{1/3} + v_{H_2O}{}^{1/3})^2}$$

$$D_{H_2-CO} = \frac{1.013\times10^{-7}T_{ct}^{1.75}[(1/M_{H_2}) + (1/M_{CO})]^{1/2}}{[P^{TPB}_{H_2} + P^{TPB}_{H_2O} + P^{TPB}_{CO} + P^{TPB}_{CO_2}](v_{H_2}{}^{1/3} + v_{CO}{}^{1/3})^2}$$

$$D_{H_2-CO_2} = \frac{1.013\times10^{-7}T_{ct}^{1.75}[(1/M_{H_2}) + (1/M_{CO_2})]^{1/2}}{[P^{TPB}_{H_2} + P^{TPB}_{H_2O} + P^{TPB}_{CO} + P^{TPB}_{CO_2}](v_{H_2}{}^{1/3} + v_{CO_2}{}^{1/3})^2}$$

$$D_{H_2O-CO} = \frac{1.013\times10^{-7}T_{ct}^{1.75}[(1/M_{H_2O}) + (1/M_{CO})]^{1/2}}{[P^{TPB}_{H_2} + P^{TPB}_{H_2O} + P^{TPB}_{CO} + P^{TPB}_{CO_2}](v_{H_2O}{}^{1/3} + v_{CO}{}^{1/3})^2}$$

$$D_{CO-CO_2} = \frac{1.013\times10^{-7}T_{ct}^{1.75}[(1/M_{CO}) + (1/M_{CO_2})]^{1/2}}{[P^{TPB}_{H_2} + P^{TPB}_{H_2O} + P^{TPB}_{CO} + P^{TPB}_{CO_2}](v_{CO}{}^{1/3} + v_{CO_2}{}^{1/3})^2}$$

ORIGINAL RESEARCH PAPER

2.4.5 Dynamic Equations for Subsystem 5 (SS5)

This subsystem (SS5) is the fuel that occupies and flows in between the space on the anode side of the cell tube. The fuel consists of CH_4, H_2O, H_2, CO, and CO_2 gases. The component mass balances on the CH_4, H_2O, H_2, CO, and CO_2 gases are given by Eqs. (44)–(51), respectively:

$$L\frac{d\rho_{fuel}^{ano}}{dt} = \rho_{fuel_{in}}^{ano}u_{fuel_{in}}^{ano} - \rho_{fuel_{in}}^{ano}u_{fuel_{in}}^{ano} + \left(\frac{2\pi r_{ct_o}L}{A_{ano}}\right)\times\begin{bmatrix} M_{H_2O}N_{H_2O} - M_{H_2}N_{H_2} + \\ M_{CO_2}N_{CO_2} - M_{CO}N_{CO}\end{bmatrix} \quad (43)$$

$$L\frac{d\left(\rho_{fuel}^{ano}\tilde{\varsigma}_{H_2}^{ano}\right)}{dt} = u_{fuel_{in}}^{ano}\rho_{fuel_{in}}^{ano}\tilde{\varsigma}_{H_{2in}}^{ano} - u_{fuel}^{ano}\rho_{fuel}^{ano}\tilde{\varsigma}_{H_2}^{ano} + \left(\frac{2\pi r_{ct_o}L}{A_{ano}}\right)M_{H_2}\left[3R_r + R_s - N_{H_2}\right] \quad (44)$$

$$L\frac{d\left(\rho_{fuel}^{ano}\tilde{\varsigma}_{H_2O}^{ano}\right)}{dt} = u_{fuel_{in}}^{ano}\rho_{fuel_{in}}^{ano}\tilde{\varsigma}_{H_2O_{in}}^{ano} - u_{fuel}^{ano}\rho_{fuel}^{ano}\tilde{\varsigma}_{H_2O}^{ano} + \left(\frac{2\pi r_{ct_o}L}{A_{ano}}\right)M_{H_2O}\left[-R_r - R_s + N_{H_2O}\right] \quad (45)$$

$$L\frac{d\left(\rho_{fuel}^{ano}\tilde{\varsigma}_{CO}^{ano}\right)}{dt} = u_{fuel_{in}}^{ano}\rho_{fuel_{in}}^{ano}\tilde{\varsigma}_{CO_{in}}^{ano} - u_{fuel}^{ano}\rho_{fuel}^{ano}\tilde{\varsigma}_{CO}^{ano} + \left(\frac{2\pi r_{ct_o}L}{A_{ano}}\right)M_{CO}[R_r - R_s - N_{CO}] \quad (46)$$

$$L\frac{d\left(\rho_{fuel}^{ano}\tilde{\varsigma}_{CH_4}^{ano}\right)}{dt} = u_{fuel_{in}}^{ano}\rho_{fuel_{in}}^{ano}\tilde{\varsigma}_{CH_{4in}}^{ano} - u_{fuel}^{ano}\rho_{fuel}^{ano}\tilde{\varsigma}_{CH_4}^{ano} + \left(\frac{2\pi r_{ct_o}L}{A_{ano}}\right)M_{H_2}[-R_r] \quad (47)$$

$$L\frac{d\left(\rho_{fuel}^{ano}\tilde{\varsigma}_{CO_2}^{ano}\right)}{dt} = u_{fuel_{in}}^{ano}\rho_{fuel_{in}}^{ano}\tilde{\varsigma}_{CO_{2in}}^{ano} - u_{fuel}^{ano}\rho_{fuel}^{ano}\tilde{\varsigma}_{CO_2}^{ano} + \left(\frac{2\pi r_{ct_o}L}{A_{ano}}\right)M_{CO_2}\left[R_s + N_{CO_2}\right] \quad (48)$$

An axial momentum balance for the fuel yields

$$L\frac{d(u_{fuel}^{ano}\rho_{fuel}^{ano})}{dt} = \left(u_{fuel_{in}}^{ano}\right)^2\rho_{fuel_{in}}^{ano} - \left(u_{fuel}^{ano}\right)^2\rho_{fuel}^{ano} + \frac{\rho_{fuel_{in}}^{ano}R^*T_{fuel_{in}}^{ano}}{M_{fuel_{in}}^{ano}} - \frac{\rho_{fuel}^{ano}R^*T_{fuel}^{ano}}{M_{fuel}^{ano}} \quad (49)$$

assuming that the wall resistance of the channel is negligible.

An energy balance for the fuel gas inside SS5 results in

$$L\frac{d(\rho_{fuel}^{ano}\tilde{H}_{fuel}^{ano})}{\partial t} = u_{fuel_{in}}^{ano}\rho_{fuel_{in}}^{ano}\tilde{H}_{fuel_{in}}^{ano} - u_{fuel}^{ano}\rho_{fuel}^{ano}\tilde{H}_{fuel}^{ano} + \frac{2r_{ct_o}Lh_{ct_o}}{A_{ano}}\left(T_{ct} - T_{fuel}^{ano}\right) + \left(\frac{2\pi r_{ct_o}L}{A_{ano}}\right)\begin{pmatrix} N_{H_2O}H_{H_2O}^{ano} - N_{H_2}H_{H_2}^{ano} \\ +N_{CO_2}H_{CO_2}^{ano} - N_{CO}H_{CO}^{ano}\end{pmatrix} - Q_{rad}^{comp} \quad (50)$$

3 Results and Discussion

3.1 Model Validation

To ensure that the model can predict the observed behavior of an operating tubular SOFC, comparison is made of the outlet voltage transient responses due to the same load step using models proposed by different researchers (see Figure 3). Qi et al. [10], have also done the same method of comparison to ensure that their model can predict the observed behavior of an operating tubular SOFC. The dynamic trend of the model presented in this work is consistent with those from other models [27, 28, 56, 57]. In this model, however, consideration has been made of not only mass, heat, and momentum transfer as well as internal reforming and shift reactions, but also of the heat sources corresponding to the reforming and shift reactions, heat produced by CO and H_2 electrochemical reactions and heat source of the radiation of fuel components. Moreover, activation and concentration losses for both CO and H_2 oxidation are also taken into account. The simulated steady state voltage from this model is lower than that calculated by others, because additional heat is absorbed by the reforming reaction and thermal radiation of gaseous components.

3.2 Effect of Thermal Radiation of Fuel Components on Fuel Cell Temperature

As is shown in Figure 4 the cell-tube temperature involving thermal radiation between fuel components and the outer cell tube is compared to same model but without accounting for this type of thermal radiation by varying the inlet fuel flow pressure. It is clearly shown that by considering the heat transfer radiation between fuel components and cell tube, the amount of cell-tube temperature is lower due to the absorption of the fuel cell energy by the fuel components by means of radiation. However, in low inlet fuel flow pressures (P_{fuelin} < 0.3 atm.) the effect of thermal radiation of fuel components on cell-tube temperature is not much significant (ΔT_{ct} < 2.6 K). On the other hand, by increasing the inlet fuel

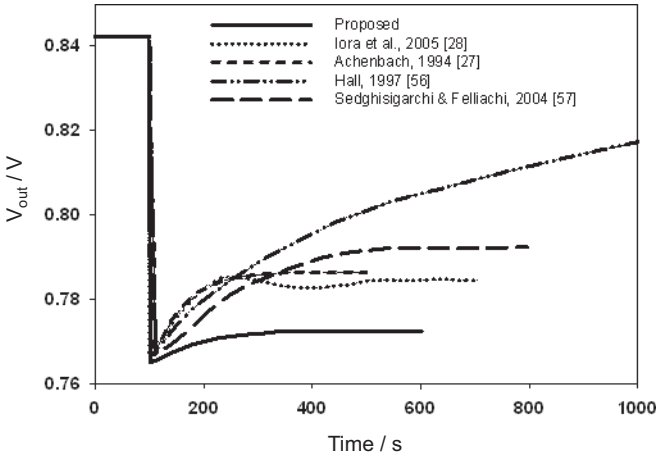

Fig. 3 Comparison of voltage responses to load step changes.

flow pressure the total emissivity of fuel gases increases thereby the effect of thermal radiation of components on cell tube temperature becomes more significant. As can be seen in Figure 4 the difference of cell tube temperature (ΔT_{ct}) for models considering fuel components with and without thermal radiation at 3 atm. of inlet fuel pressure is 5 K.

It is shown in Figure 5 that when the length of cell-tube is smaller than 0.02 m, the effect of thermal radiation of fuel components on fuel cell temperature is minor and negligible while in larger cell-tube lengths its effect becomes more important. This is because the larger cell-tube length implies larger heat exchange area, resulting in an increase in the total emissivity of fuel gases thereby resulting in the absorption of more fuel cell energy by means of thermal radiation of fuel components.

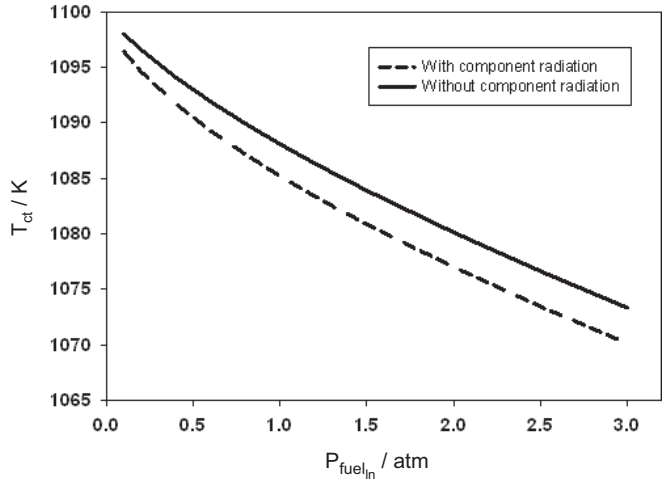

Fig. 4 Comparison of the cell-tube temperature involving thermal radiation between fuel components and the outer cell tube with that model that does not account for this type of thermal radiation in response to the variation of the inlet fuel flow pressure.

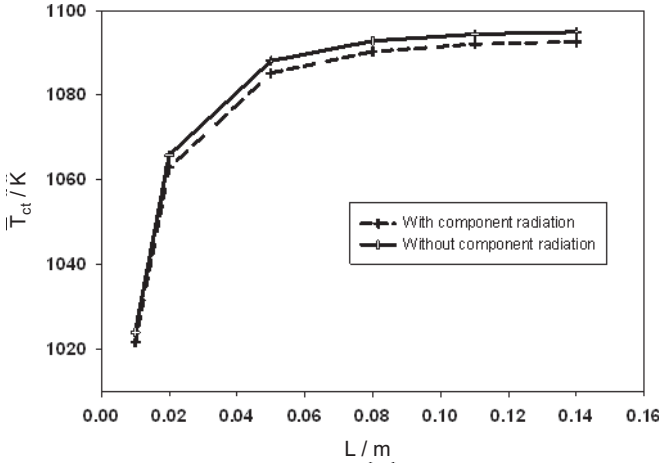

Fig. 5 Comparison of the cell-tube temperature involving thermal radiation between fuel components and the outer cell tube with that model that does not account for thermal radiation in response to the variation of the fuel cell length.

3.3 *Effect of CO Electrochemical Reaction on Fuel Cell Performance*

It is shown in Figure 6 that by considering the CO electrochemical reaction the performance of the SOFC is better than the model that has ignored this reaction. This is because the current is produced by the sum of hydrogen and carbon monoxide oxidation at the anodic side by the electrochemical reaction, while in the model that does not consider the CO electrochemical reaction, it is assumed that the current is produced only by the H_2 oxidation. In addition, the CO and CO_2 diffusion into the anode and fuel channel is not considered in the model that does not consider the CO electrochemical reaction, respectively. As a result, the anodic side activation and concentration polarizations of the model that considers the CO electrochemical reaction, are lower than the model that ignores the CO electrochemical reaction. Therefore, the outlet voltage of the model involving the CO electrochemical reaction is 0.36% higher in comparison to the model that neglects the CO electrochemical reaction.

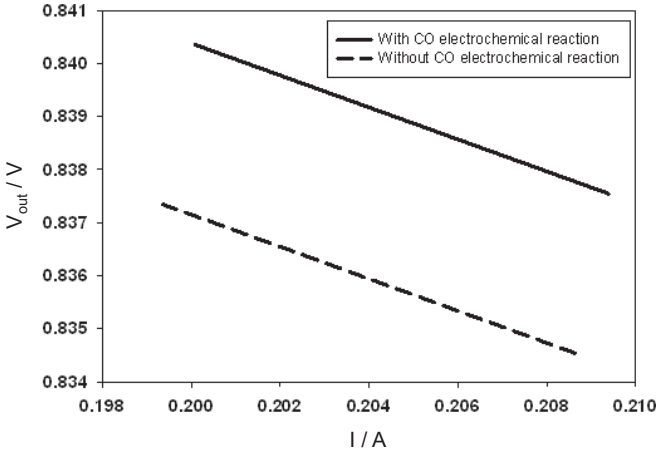

Fig. 6 Comparison of the performance of the SOFC model with and without the inclusion of the CO electrochemical reaction.

Reforming reaction highly depends on fuel flow pressure therefore, in high fuel flow pressure the reaction rate increases while the amount of H_2 produced is 3 times greater than that produced by CO from this reaction. Due to higher H_2 concentration compared to CO, the hydrogen electrochemical reaction dominates over the CO electrochemical reaction and therefore more current is produced by H_2 oxidation. This is why in high fuel flow pressures; the consideration of the CO electrochemical reaction is less important (see Figure 7). Based on the results, in more than 2 atm. of fuel flow pressures the role of CO electrochemical reaction is insignificant where it is clearly shown in Figure 7 that at lower inlet fuel flow pressure, CO electrochemical reaction is significant to consider along with H_2 oxidation. Shift and reforming reactions highly depend on fuel flow pressure. That is why in lower fuel flow pressures the rate of shift and reforming reactions reduce. Therefore less CO inside the fuel

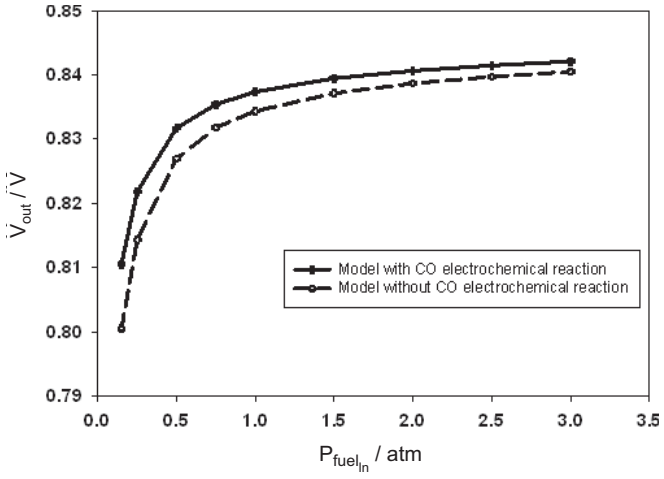

Fig. 7 Comparison of the outlet cell voltage for models with and without the consideration of the CO electrochemical reaction in response to changes in the inlet fuel flow pressure.

is consumed by the shift reaction and also less H_2 is produced by the reforming reaction. In this situation the CO and H_2 electrochemical reactions are competitive.

As can be seen in Figure 8 by enhancing the CO/H_2 ratio the fuel cell outlet voltage increases. It is observed that CO improves the SOFC performance while it is considered as a poison component at low fuel cell temperatures. In fact, the activation polarization depends on the CO concentration and decreases when the amount of CO in fuel increases. It is clearly shown in the same figure that in high CO/H_2 ratio the role of CO electrochemical reaction becomes more important due to high the CO concentrations. When the concentration of CO in fuel increases the rate of reforming reaction decreases thereby resulting in less H_2 production by the reaction. Therefore, CO oxidation becomes compatible with H_2 oxidation inside the TPB.

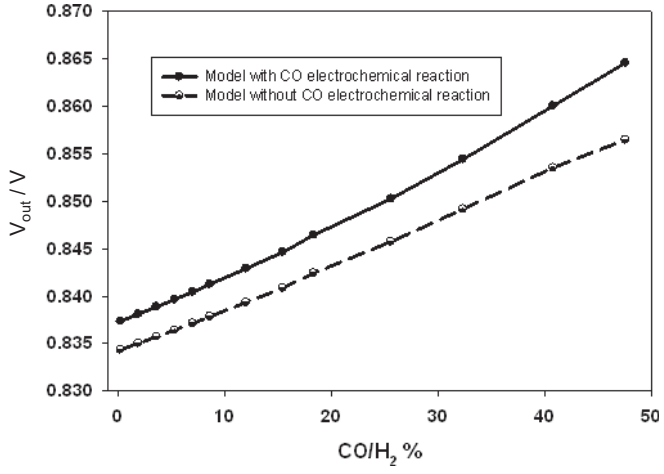

Fig. 8 Comparison of the outlet cell voltage for models with and without the consideration of the CO electrochemical reaction in response to changes in the CO/H_2 ratio.

4 Summary

A dynamic model of a tubular SOFC is presented in this work. The model accounts for diffusion processes, inherent impedance, transport (momentum, heat and mass transfer) processes, electrochemical processes including hydrogen and carbon monoxide oxidations, anodic and cathode activation/concentration polarizations and ohmic losses, and internal reforming/shifting reactions, among others. Simulation results indicate that at higher inlet fuel flow pressures and also larger fuel cell lengths the effect of thermal radiation of gaseous components on fuel cell temperature becomes more significant. However, the importance of thermal radiation of gaseous components at high fuel flow pressures is more significant than the influence of the length of the cell-tube.

It is also observed that in the same fuel cell operating conditions the performance of the SOFC for the model that considers the CO electrochemical reaction is higher than that of the model that does not consider this reaction. Moreover, at low inlet fuel flow pressures the CO electrochemical reaction is comparable with the H_2 electrochemical reaction and significant enough to account for in the model. The results show that by enhancing the CO/H_2 ratio the fuel cell performance increases and CO oxidation becomes comparable with H_2 oxidation inside the TPB.

Acknowledgement

The authors are grateful to the UM Bright Sparks Unit (Bsp_App462/11(K)) and the UM/MOHE High Impact Research Grant (UM.C/HIR/MOHE/ENG/18) for providing financial assistance during this work.

List of Symbols

A_{ano}	Anode-side flow-channel cross-sectional area (m^2)
C_{ct}	Charge transfer capacity (F; note that 1 F = 1 A s V^{-1})
C_p	Specific heat capacity at constant pressure (kJ/(kmol K))
$\bar{C}_p$	Specific heat capacity at constant pressure (kJ/(kg K))
C_v	Specific heat capacity at constant volume (kJ/(kmol K))
$\bar{C}_v$	Specific heat capacity at constant volume (kJ/(kg K))
D	Total diffusion coefficient (m^2 s^{-1})
E	Irreversible cell voltage (V)
E_{rev}	Reversible cell voltage (V)
$E_{act_{ano}}$	Activation energy of anode (kJ $kmol^{-1}$)
$E_{act_{cat}}$	Activation energy of cathode (kJ $kmol^{-1}$)
E_r	Activation energy of ammonia decomposition (kJ $kmol^{-1}$)
h	Convective film heat-transfer coefficient (kJ/(s m^2 K))
H	Enthalpy of formation (kJ $kmol^{-1}$)
$\bar{H}$	Enthalpy of formation (kJ kg^{-1})

I	Cell current (A)
i	Current density (A cm^{-2})
L	Length of the tubular fuel cell (length of the cell and injection tubes) (m)
m	Mass (kg)
M	Molecular weight (kg $kmol^{-1}$)
N	Rate of mass transfer (kmol/(s m^2))
p	Partial pressure (atm)
P	Total pressure (atm)
r	Radius (m)
R	Universal gas constant; $R = 8.20575 \times 10^{-2}$ m^3 atm/(K kmol)
R^*	Universal gas constant; $R^* = 8.31447 \times 10^3$ m^2 kg/(K kmol s^2)
R_J	Universal gas constant; $R_J = 8.31447 \times 10^3$ J/(K kmol)
R_{kJ}	Universal gas constant; $R_{kJ} = 8.31447$ kJ/(K kmol)
R_{load}	External load resistance (Ω)
R_r	Rate of reforming reaction (kmol s m^{-2})
R_{Rad}	Radiative heat transfer resistance
R_{tct}	Total charge transfer resistance (Ω)
R_{to}	Total ohmic resistance (Ω)
R_{H2}	Rate of consumption of H_2 (kmol s^{-1})
R_{H2O}	Rate of consumption of H_2O (kmol s^{-1})
R_{O2}	Rate of consumption of O_2 (kmol s^{-1})
T	Temperature (K)
u	Fluid velocity (m s^{-1})
V_{out}	Fuel-cell outlet voltage (V)
z_r	Frequency factor of the ammonia decomposition (kmol/$atm^{0.5}$ m^2 s)

Greek Letters

Δ	Thickness of the diffusion layer (m)
δ	Mean pore radius (m)
ε	Porosity
ρ	Density (kg m^{-3})
$\tilde{\zeta}$	Mass fraction
ζ	Mole fraction
τ	Tortuosity

Superscripts

ano	Anode
Cat	Cathode
inj	Injection tube
TPB	Triple phase boundary

Subscript

air	Air
ano	Anode
cat	Cathode
ct	Cell tube
fuel	Fuel
it	Injection tube
i	Inner
in	Inlet
load	Load
o	Outer
out	Output
tct	Total charge transfer
to	Total ohmic

References

[1] R. Suwanwarangkul, E. Croiset, M. W. Fowler, P. L. Douglas, E. Entchev, M. A. Douglas, *J. Power Sources* **2003**, *122*, 9.
[2] M. H. Chakrabarti, E. P. L. Roberts, *NED Univ. J. Res.* **2008**, *5*, 43.
[3] M. A. Khaleel, Z. Lin, P. Singh, W. Surdoval, D. Collin, *J. Power Sources* **2004**, *130*, 136.
[4] S. A. Hajimolana, M. A. Hussain, W. M. A. W. Daud, M. Soroush, A. Shamiri, *Renewable Sustainable Energy Rev.* **2011**, *15*, 1893.
[5] S. A. Hajimolana, M. A. Hussain, W. M. A. W. Daud, M. H. Chakrabarti, *Chem. Eng. Res. Des.*, DOI: 10.1016/j.cherd.2012.03.004
[6] L. Liu, R. Flesner, G. Y. Kim, A. Chandra, *Fuel Cells* **2012**, *12*, 97.
[7] S. Bozorgmehri, M. Hamedi, *Fuel Cells* **2012**, *12*, 11.
[8] S. Lin, J. Selig, in *Advanced Processing and Manufacturing Technologies for Structural and Multifunctional Materials II: Ceramic Engineering and Science Proceedings, Volume 29, Issue 9*, John Wiley & Sons, Inc., New York, USA, **2009**, pp. 53.
[9] H. Yakabe, M. Hishinuma, M. Uratani, Y. Matsuzaki, I. Yasuda, *J. Power Sources* **2000**, *86*, 423.
[10] Y. Qi, B. Huang, J. Luo, *Chem. Eng. Sci.* **2006**, *61*, 6057.
[11] S. H. Chan, K. A. Khor, Z. T. Xia, *J. Power Sources* **2001**, *93*, 130.
[12] A. Chaisantikulwat, C. Diaz-Goano, E. S. Meadows, *Comput. Chem. Eng.* **2008**, *32*, 2365.
[13] S. Nagata, A. Momma, T. Kato, Y. Kasuga, *J. Power Sources* **2001**, *101*, 60.
[14] M. M. Hussain, X. Li, I. Dincer, *J. Power Sources* **2009**, *189*, 916.
[15] R. Bove, S. Ubertini, *J. Power Sources* **2006**, *159*, 543.
[16] J. R. Izzo Jr., A. A. Peracchio, W. K. S. Chiu, *J. Power Sources* **2008**, *176*, 200.
[17] F. N. Cayan, S. R. Pakalapati, F. Elizalde-Blancas, I. Celik, *J. Power Sources* **2009**, *192*, 467.
[18] T. X. Ho, P. Kosinski, A. C. Hoffmann, A. Vik, *Chem. Eng. Sci.* **2008**, *63*, 5356.
[19] T. X. Ho, P. Kosinski, A. C. Hoffmann, A. Vik, *Int. J. Hydrogen Energy* **2009**, *34*, 3488.
[20] M. Ni, D. Y. C. Leung, M. K. H. Leung, *J. Power Sources* **2008**, *183*, 668.
[21] K. Nikooyeh, A. A. Jeje, J. M. Hill, *J. Power Sources* **2007**, *171*, 601.

[22] B. Morel, J. Laurencin, Y. Bultel, F. Lefebvre-Joud, *J. Electrochem. Soc.* **2005**, *152*, 1382.
[23] J. R. Ferguson, J. M. Fiard, R. Herbin, *J. Power Sources* **1996**, *58*, 109.
[24] R. Suwanwarangkul, E. Croiset, M. D. Pritzker, M. W. Fowler, P. L. Douglas, E. Entchev, *J. Power Sources* **2007**, *166*, 386.
[25] M. Karcz, *Energy Convers. Manage.* **2009**, *50*, 2307.
[26] S. Hajimolana, M. Soroush, *Ind. Eng. Chem. Res.* **2009**, *48*, 6112.
[27] E. Achenbach, *J. Power Sources* **1994**, *49*, 333.
[28] P. Iora, P. Aguiar, C. S. Adjimanb, N. P. Brandon, *Chem. Eng. Sci.* **2005**, *60*, 2963.
[29] S. Campanari, P. Iora, *J. Power Sources* **2004**, *132*, 113.
[30] P. Aguiar, C. S. Adjiman, N. P. Brandon, *J. Power Sources* **2004**, *138*, 120.
[31] A. V. Virkar, *Ph.D. Thesis*, University of Utah **2000**.
[32] M. Bavarian, M. Soroush, *Chem. Eng. Sci.* **2011**, *67*, 2.
[33] Z. Ma, *Ph.D. Thesis*, Georgia Institute of Technology, Georgia, **2000**.
[34] M. F. Modest, *Radiative Heat Transfer*, 2nd Ed., Academic Press, New York, USA, **2003**.
[35] N. F. Bessette, W. J. Wepfer, *Energy Convers. Manage.* **1996**, *37*, 281.
[36] P. Costamagna, P. Costa, V. Antonucci, *Electrochim. Acta* **1998**, *43*, 375.
[37] C. Stiller, B. Thorud, S. Seljebø, Ø. Mathisen, H. Karoliussen, O. Bolland, *J. Power Sources* **2005**, *141*, 227.
[38] B. A. Haberman, J. B. Young, *Int. J. Heat Mass Transfer* **2004**, *47*, 3617.
[39] F. P. Nagel, T. J. Schildhauer, S. M. A. Biollaz, A. Wokaun, *J. Power Sources* **2008**, *184*, 143.
[40] M. M. Hussain, X. Li, I. Dincer, *J. Power Sources* **2006**, *161*, 1012.
[41] A. Salogni, P. Colonna, *Appl. Therm. Eng.* **2009**, *30*, 464.
[42] U. Doraswami, N. Droushiotis, G. H. Kelsall, *Electrochim. Acta* **2010**, *55*, 3766.
[43] M. Ni, *Energy Convers. Manage.* **2010**, *51*, 714.
[44] K. P. Recknagle, E. M. Ryan, B. J. Koeppel, L. A. Mahoney, M. A. Khaleel, *J. Power Sources* **2004**, *195*, 6637.
[45] N. Akhtar, S. P. Decent, K. Kendall, *J. Power Sources* **2010**, *195*, 7796.
[46] P. Hofmann, K. D. Panopoulos, L. E. Fryda, E. Kakaras, *Energy* **2009**, *34*, 2151.
[47] L. Petruzzi, S. Cocchi, F. Fineschi, *J. Power Sources* **2003**, *118*, 96.
[48] T. Aloui, K. Halouani, *Appl. Therm. Eng.* **2007**, *27*, 731.
[49] P. S. Cumber, M. Fairweather, *Int. J. Heat Mass Transfer* **2005**, *48*, 5221.
[50] J. S. Truelove, *AERE-R8494*, *UKAEA*, *Harwell*, **1976**.
[51] M. F. Modest, *J. Heat Transfer* **1991**, *113*, 650.
[52] D. B. Olfe, *Ph.D. Thesis*, California Institute of Technology, Pasadena, California **1960**.
[53] P. Li, M. Chyu, *Heat Transfer Trans. ASME* **2005**, *127*, 1344.
[54] Y. Qi, B. Huang, K. T. Chuang, *J. Power Sources* **2005**, *150*, 32.
[55] J. R. W. Welty, C. E. Wilson, R. E. Rorrer, 4th Ed., Wiley, New York **2000**.
[56] D. J. Hall, *Ph. D. Thesis*, University of Pittsburgh, **1997**.
[57] K. Sedghisigarchi, A. Feliachi, *IEEE Trans. Energy Convers.* **2004**, *19*, 423.
[58] R. B. Bird, W. E. Stewart, E. N. Lightfoot, *Transport Phenomena*, 2nd Ed., John Wiley & Sons Inc., New York, USA, **2007**.
[59] I. K. Kookos, *Chem. Eng. Sci.* **2012**, *69*, 571.

